JPE 17-1-30

https://doi.org/10.6113/JPE.2017.17.1.305
ISSN(Print): 1598-2092 / ISSN(Online): 2093-4718

An Interference Isolation Method for Wireless Power and Signal Parallel Transmissions on CPT Systems

Wei Zhou*, Yu-Gang Su†,*, Shi-Yun Xie*, Long Chen*, Xin Dai*, and Yu-Ming Zhao*

†State Key Laboratory of Power Transmission Equipment and System Security and New Technology, Chongqing University, Chongqing, China
*College of Automation, Chongqing University, Chongqing, China

Abstract

A novel interference isolation method is proposed by using several designed coils in capacitive power transfer systems as isolation impedances. For each designed coil, its stray parameters such as the inter-turn capacitance, coil resistance and capacitance between the coil and the core, etc. are taken into account. An equivalent circuit model of the designed coil is established. According to this equivalent circuit, the impedance characteristic of the coil is calculated. In addition, the maximum impedance point and the corresponding excitation frequency of the coil are obtained. Based on this analysis, six designed coils are adopted to isolate the interference from power delivery. The proposed method is verified through experiments with a power carrier frequency of 1MHz and a data carrier frequency of 8.7MHz. The power and data are transferred parrallelly with a data carrier attenuation lower than -5dB and a power attenuation on the sensing resistor higher than -45dB.

Key words: Capacitive power transfer (CPT), Coil stray parameters, Interference isolation, Wireless power and signal parallel transmission

I. INTRODUCTION

In recent years, wireless power transfer (WPT) technologies have been widely adopted in practical applications as a solution for power transfer without a direct wire connection [1]-[4]. As a kind of transmission mode, capacitive power transfer (CPT, or capacitively coupled power transfer, CCPT) technologies [5], [6] are attracting a growing number of researchers due to their advantages such as design flexibility, reduced volume and weight of the coupling structure and metal penetration capability [7], [8] because capacitive plates are utilized as the coupling structure. CPT technologies have been used in rotating devices [9], mobile robots [10], biological implants [11], cell phones [12], and electric vehicles [13], [14].

Many CPT studies have focused on improving the power transfer efficiency and the power level of the whole CPT system [15]-[17]. To achieve both of the above targets, wireless data transmission between the power transmitter and receiver is brought into CPT systems which forms a combined system referred to as a wireless power and signal parallel transmission (WPST) system. In addition, this system can also be used in certain applications such as medical implants and consumer electronics, which need to transfer sensor data, control signals, etc.

Generally, the transmission methods of a WPST system include the dual channel method [18] and the shared channel method [19], which are shown in Fig. 1. For the second method, the power carrier and data carrier transfer in a single shared channel, and only one coupling structure is set in the system which can simplify the system complexity and enhance the flexibility of the coupling structure. However, in a WPST system with a shared channel, the power carrier from the input Port A seriously interferes with the data channel. Therefore, it is important to isolate the crosstalk between the power and data carriers. In the existing studies, some isolation strategies have been adopted. Wu, et al. isolated interference by reducing the signal coupling inductances and magnifying the data carrier, while more power is consumed by the data transmission [20]. Hairi, et al. tried to send and receive data during the inverter non-switching period in synchronization with the rising or

Manuscript received Mar. 18, 2016; accepted Nov. 14, 2016
Recommended for publication by Associate Editor Jee-Hoon Jung.
†Corresponding Author: su7558@qq.com
Tel: +86-23-65112750, Fax: +86-23-65111221, Chongqing University
*College of Automation, Chongqing University, China

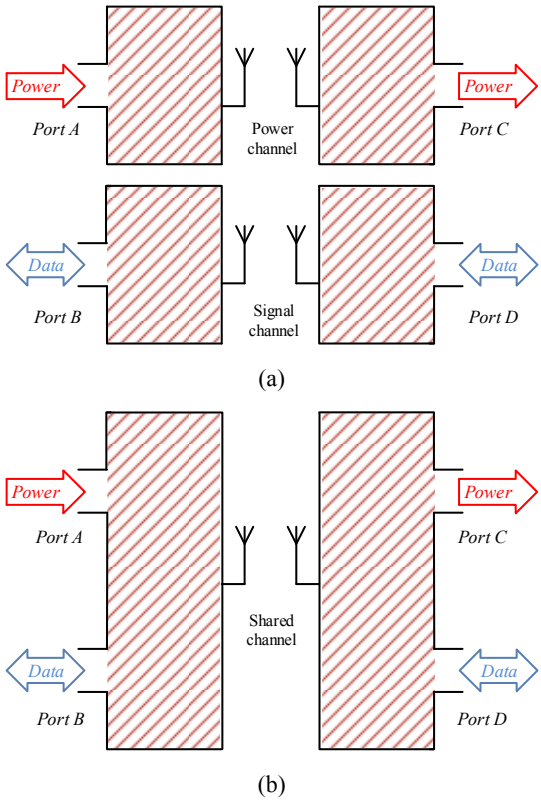

Fig. 1. Two transmission methods of the WPST system include: (a) the dual channels method and (b) the shared channel method.

falling edge of the inverter voltage to avoid the power interference on the data link [21]. However, the maximum baud rate was seriously limited by the switching frequency of the inverter.

In this paper, a novel interference isolation method is proposed by using several designed coils in a CPT system as isolation impedances. For each designed coil, the stray parameters such as the inter-turn capacitance, coil resistance, capacitance between the coil and the core, etc. are taken into account and an equivalent circuit model of the designed coils is established. According to the equivalent circuit, the maximum impedance point of each coil and the maximum impedance frequency (MIF) are calculated. Based on the characteristics of the equivalent circuit model, six designed coils are adopted to isolate the interference from power delivery.

II. Interference and Carrier Gain Modeling

Fig. 2 shows a typical topology of a CPT system. The full-bridge inverter transforms DC voltage E_{dc} into a high frequency AC voltage which is referred to as u_p. The combination of a DC source E_{dc} and a full-bridge inverter can be regarded as an AC voltage source u_p. C_{s1} and C_{s2} indicate the equivalent capacitors of two pairs of capacitive coupling plates. The tuning inductors L_{st} and L_{sr} are both connected in series with C_{s1} and C_{s2} to compensate the reactive power

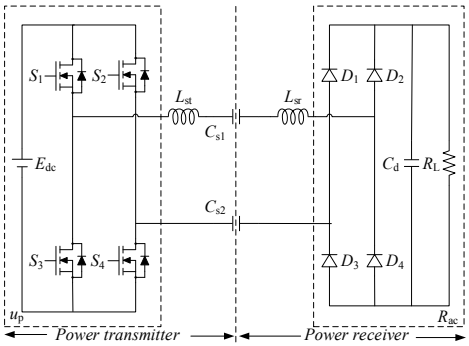

Fig. 2. Typical topology of the CPT system.

circulation in the resonant circuit. A full-bridge rectifier with four diodes D_1-D_4 transforms AC voltage into a DC voltage to directly supply the load R_L. An equivalent AC resistance R_{ac} is used to replace the rectifier, filter capacitor C_d, and load R_L to simplify the analysis [22].

A WPST equivalent circuit based on a typical CPT topology is shown in Fig. 3. A couple of data branches are connected in parallel to the capacitive plates on both sides. Each data branch has two operation modes, the transmitter mode and the receiver mode, which are controlled by the switches S_t and S_r. Under the transmitter mode, the carrier generator and the data modulation circuit are switched on and form a data source u_{td} or u_{rd} to transmit data. Under the receiver mode, a sensing resistor R_{td} or R_{rd} is connected to the main circuit to receive data. From Fig. 3(a), two serious interference voltages u_{AB} and u_{CD} are added directly to the data sensing resistors R_{td} and R_{rd} if there are no isolation modules. Under this condition, the received data will be easily lost in the power interference, even if there is a big difference between the frequencies of the power carrier and the data carrier. Therefore, a WPST system with four isolation impedances is proposed and shown in Fig. 3(b) to separate the power carrier and data carrier.

In order to prevent serious power interference, the impedances Z_{t2} and Z_{r2} have to be large enough under the operating frequency of the power transmission. In addition, a high impedance can also prevent power loss on the data branches to maintain the power efficiency. Conversely, Z_{t2} and Z_{r2} have to be small enough under the frequency of the data carrier to ensure that the data can be transferred through them without a serious attenuation. The impedances Z_{t1} and Z_{r1} are designed based on the inductors L_{st} and L_{sr} in the original CPT circuit. The impedances Z_{t1} and Z_{r1} have to be set large enough under the data carrier frequency to ensure that the data carrier can transfer across the coupling capacitors as much as possible to increase the voltage gain of the data carrier in the data channel. In addition, the impedances of Z_{t1} and Z_{r1} compensate the reactive power circulation of the coupling capacitors under the power operating frequency.

In order to analyze the wireless power and signal transfer

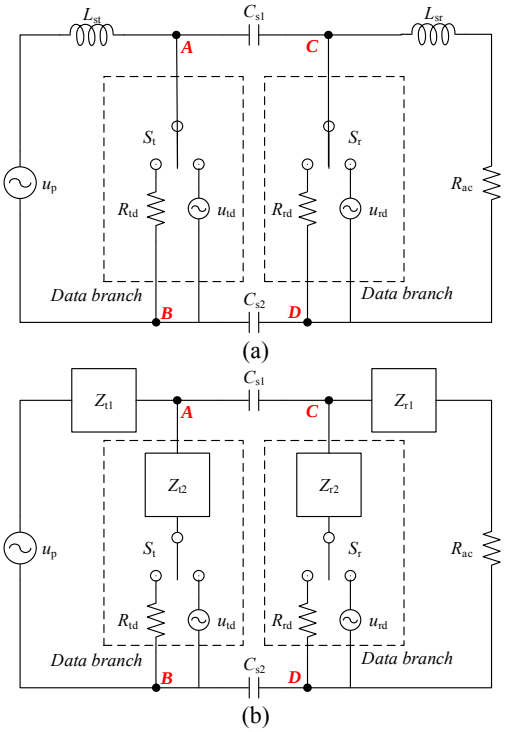

Fig. 3. Equivalent circuits of the WPST system with/without isolation modules: (a) the equivalent circuit of WPST system without isolation impedances and (b) the equivalent circuit of WPST system with isolation impedances.

characteristics, five voltage gain functions are derived and shown in the Appendix as Eq.(14) to Eq.(18). Firstly, the functions $G_{\text{int-tr}}$ and $G_{\text{int-rt}}$ in Eq.(14) and Eq.(15), which represent the voltage gains from the input power source u_p to the noise voltage on the sensing resistors R_{rd} and R_{td}, are obtained to ensure that the data carrier can be recognized from the power interference. Moreover, in order to clearly distinguish data bit 0 and data bit 1 in the ASK demodulation, the functions $G_{\text{gain-tr}}$ and $G_{\text{gain-rt}}$ in Eq.(16) and Eq.(17), which indicate the data carrier gains from the two data sources to the received voltages on the sensing resistors, are given. Here the function $G_{\text{gain-tr}}$ means the data carrier gain when the data transfers forward from the power transmitter to the receiver, and the function $G_{\text{gain-rt}}$ presents the carrier gain in the backward condition. To maintain the power transfer capacity of a CPT system with two signal branches, the function G_{power} in Eq.(18) is derived to express the power voltage gain from the input power source u_p to the load R_{ac}.

III. Coils Equivalent Circuit and Modeling

To transfer data with a high carrier voltage gain and a low power interference, four impedance modules Z_{t1}, Z_{t2}, Z_{r1} and Z_{r2} should be replaced by some designed coils. The impedances of these coils are calculated in this section.

A. Coil Parameters

For the designed coils, each turn of the winding can be regarded as a rectangular ring conductor with a wire radius of r and ring side lengths of a and b. The self-inductance L_t of each turn of the windings can be indicated as:

$$L_t = \frac{\mu}{\pi}\left(a\ln\frac{2ab}{r(a+b)} + b\ln\frac{2ab}{r(b+d)} - \frac{3(a+b)}{4} + 2d\right) \quad (1)$$

where $d=\sqrt{a^2+b^2}$, μ represents the permeability of the core. Moreover, because the magnetic circuit in the ring core is closed, the coefficient of the mutual inductance between each turn is nearly 1. Therefore, the mutual inductance M_{ij} between the i^{th} and j^{th} turns is equal to the self-inductor of a single turn L_t. For the n^{th} turn, the sum of the mutual inductances between all of the other turns with the n^{th} turn and the self-inductance of the n^{th} turn is equivalent to a current-controlled voltage source u_{lt} which is shown in Fig. 4.

$$u_{lt} = j\omega L_t \sum_{n=1}^{N} i_{rtn} \quad (2)$$

Beside the self-inductance, the other main stray parameters considered in this paper include the inter-turn capacitance, the capacitance between the coil and the core, the coil resistance and the core resistance.

Fig. 4 shows an equivalent circuit diagram of the designed coil considering these stray parameters.

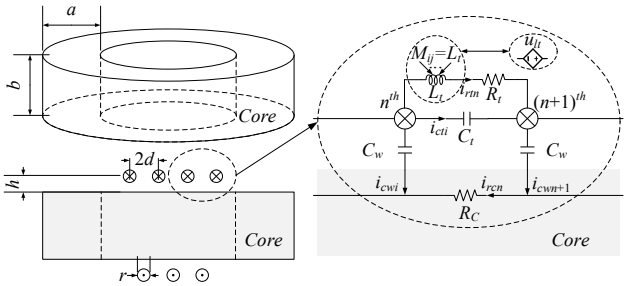

Fig. 4. Equivalent circuit diagram of the designed coil with stray parameters.

The distributed stray capacitance from each turn of the windings to the core is approximated as a circular conductor at a distance of h over the ground plane as:

$$C_w = \frac{4\pi\varepsilon_0(a+b)}{\ln\left(h/r+\sqrt{(h/r)^2-1}\right)} \quad (3)$$

where ε_0 represents the permittivity of vacuum. Moreover, the inter-turn capacitance between adjacent windings is approximately equivalent to two ring conductors with a distance of $2d$ and is expressed as:

$$C_t = \frac{2\pi\varepsilon_0(a+b)}{\ln\left(d/r+\sqrt{(d/r)^2-1}\right)} \quad (4)$$

Generally, compared with the stray capacitance C_w, the inter-turn capacitance C_t can be ignored due to the relatively large d.

The internal resistance of the designed coil windings is modeled as a circular cross-sectional wire resistance including the skin effect, which is given as below:

$$R_t = \frac{\rho L}{S} = \frac{2(a+b)\rho}{\pi r^2 - \pi(r-\Delta r)^2} \tag{5}$$

where ρ indicates the resistivity, L is the wire length of a single winding, S represents the effective area of the current flow, and Δr means the skin depth. The core resistance R_c is determined by the magnetic core material, and the resistance value is given by actual measurement.

B. Equivalent Model and the Coil Impedance

According to the equivalent circuit of a single winding in Fig. 4, the equivalent circuit of the designed coil can be established by cascading all of the equivalent circuits of each winding. Then the model of the designed coil is given by setting up the Kirchhoff's Voltage Law (KVL) equation group with $2N$+1 equations and the Kirchhoff's current law (KCL) equation group with $2N$-1 equations as below:

$$\begin{cases} \left.\begin{aligned} -i_{rtn-1} + i_{rtn} - i_{ctn-1} + i_{ctn} + i_{cwn} = 0 \quad & n \in [2, N] \\ i_{cwn} - i_{rcn-1} + i_{rcn} = 0 \quad & n \in [2, N] \\ i_{in} - i_{rt1} - i_{ct1} + i_{rc1} = 0 & \end{aligned}\right\} KCL \\ \left.\begin{aligned} i_{rtn} R_t - i_{ctn} Z_{ct} + u_{lt} = 0 \quad & n \in [1, N] \\ i_{ctn} Z_{ct} - i_{cwn} Z_{cw} + i_{cwn+1} Z_{cw} + i_{rcn} R_c = 0 \quad & n \in [2, N-1] \\ i_{ct1} Z_{ct} + i_{rc1}(Z_{cw} + R_c) + i_{cw2} Z_{cw} = 0 & \\ i_{ctN} Z_{ct} + i_{rcN}(Z_{cw} + R_c) - i_{cwN} Z_{cw} = 0 & \\ R_t \sum_{k=1}^{N} i_{rtk} + N u_{lt} = u_{in} & \end{aligned}\right\} KVL \end{cases} \tag{6}$$

where i_{rtn}, i_{ctn}, i_{cwn} and i_{rcn} represent the current of R_t, C_t, C_w and R_c of the n^{th} winding of the coil, respectively. u_{in} and i_{in} are expressed as the input voltage and current of the coils. N is the number of coil turns. Z_{ct} and Z_{cw} represent the impedances of the capacitances C_t and C_w, respectively.

To obtain a convenient calculation, the KVL and KCL equation groups with $4N$ equations are transformed into a $4N$-order matrix function as below:

$$\begin{cases} \mathbf{A}_{4N\times 4N} x + \mathbf{B}_{4N\times 1} u_{lt} = \mathbf{C}_{4N\times 1} u_{in} \\ u_{lt} = \mathbf{D}_{1\times 4N} x \end{cases} \tag{7}$$

where:

$$x = \left(i_{in},\ \mathbf{i}_{rtP},\ \mathbf{i}_{ctQ},\ \mathbf{i}_{rcS},\ \mathbf{i}_{cwT}\right)^T,$$

$$\mathbf{A} = \left(\begin{array}{c|c|c|cc|c} 1 & \multirow{2}{*}{$\mathbf{A}_1$} & \multirow{2}{*}{$\mathbf{A}_1$} & 1 & $\mathbf{0}_{1\times N-1}$ & $\mathbf{0}_{1\times N-1}$ \\ $\mathbf{0}_{N-1\times 1}$ & & & \multicolumn{2}{c|}{$\mathbf{0}_{N-1\times N}$} & $-\mathbf{I}_{N-1}$ \\ \hline $\mathbf{0}_{N-1\times 1}$ & $\mathbf{0}_{N-1\times N}$ & $\mathbf{0}_{N-1\times N}$ & \multicolumn{2}{c|}{$\begin{matrix} 1 & -1 & & \\ & \ddots & \ddots & \\ & & 1 & -1 \end{matrix}$} & $-\mathbf{I}_{N-1}$ \\ \hline $\mathbf{0}_{N\times 1}$ & $R_t \times \mathbf{I}_N$ & $-Z_{ct} \times \mathbf{I}_N$ & \multicolumn{2}{c|}{$\mathbf{0}_N$} & $\mathbf{0}_{N\times N-1}$ \\ \hline $\mathbf{0}_{N+1\times 1}$ & $\begin{matrix} \mathbf{0}_N \\ R_t \times \mathbf{1}_{1\times N} \end{matrix}$ & $\begin{matrix} Z_{ct} \times \mathbf{I}_N \\ \mathbf{0}_{1\times N} \end{matrix}$ & \multicolumn{2}{c|}{$\mathbf{A}_2$} & $\mathbf{A}_3$ \end{array}\right),$$

$$\mathbf{B} = \left(\mathbf{0}_{1\times 2N-1} \quad \mathbf{1}_{1\times N} \quad \mathbf{0}_{1\times N} \quad N\right)^T, \mathbf{C} = \left(0_{1\times 4N-1} \quad 1\right)^T,$$

$$\mathbf{D} = \left(0 \quad Z_{lt} \times \mathbf{1}_{1\times N} \quad \mathbf{0}_{1\times 3N-1}\right), \mathbf{A}_1 = \begin{pmatrix} -1 & & & \\ 1 & \ddots & & \\ & \ddots & \ddots & \\ & & 1 & -1 \end{pmatrix},$$

$$\mathbf{A}_2 = \begin{pmatrix} R_c + Z_{cw} & & & \\ & R_c \times \mathbf{I}_{N-2} & & \\ & & & R_c + Z_{cw} \\ 0 & \cdots & & 0 \end{pmatrix},$$

$$\mathbf{A}_3 = \begin{pmatrix} Z_{cw} & & & \\ -Z_{cw} & \ddots & & \\ & \ddots & Z_{cw} & \\ & & -Z_{cw} & \\ 0 & \cdots & 0 & \end{pmatrix},$$

where P=[1, N]∈ℵ, Q=[1, N]∈ℵ, S=[1, N]∈ℵ, T=[1, N]∈ℵ, and ℵ presents the set of the integer. The designed coil impedances can be calculated according to Eq.(8) as follows:

$$Z_{coil} = \frac{u_{in}}{i_{in}} = \left(\mathbf{Y}\left(\mathbf{A} + \mathbf{BD}\right)^{-1}\mathbf{C}\right)^{-1} \tag{8}$$

where $\mathbf{Y}$=(1, 0, 0, ⋯, 0, 0)$_{1\times 4N}$.

IV. Frequency-domain Analysis of the Coils and Interference Isolation

According to the modeling of the designed coil, the impedance of the coil is accurately calculated. From Section III, the coil impedance is influenced by the coil turn number N, the operating frequency ω, and the coil geometric parameters such as a and b, etc.

A. Frequency-Domain Analysis of the Coils

The geometric parameters of the coil in Section III include the ring side lengths a and b, the wire radius r, the turn distance d, and the distance between windings and the core h. To simplify the analysis, a (assume a=b), d, and h are set as constants by choosing a specific wire and winding method. Only the parameter r is considered as a variable in the following analysis. Therefore, the coil impedance can be expressed as a function with the variables a, N, and f as in $Z_{coil}(a, N, f)$.

Fig. 5 shows the impedance characteristic of the designed coil in the frequency domain. Due to stray parameters, the coil impedance appears in the inductive reactance in the low frequency region and in the capacitive reactance in the high frequency region. The total impedance achieves its peak value on the demarcation point of these two regions and the frequency of the demarcation point is defined as the maximum impedance frequency (MIF). Fig. 6 shows a contour plot of the MIF, where the side length of core a varies from 0.3cm-2cm and the coil turn number variation ranges from 5 to 95. From Fig. 6, it can be seen that the MIFs can be achieved from 1MHz to 9MHz by setting the core radius r and the turn number N in a specific region. The maximum impedance in the MIF point can be designed to isolate the power interference and to keep the data carrier transferring through data branches.

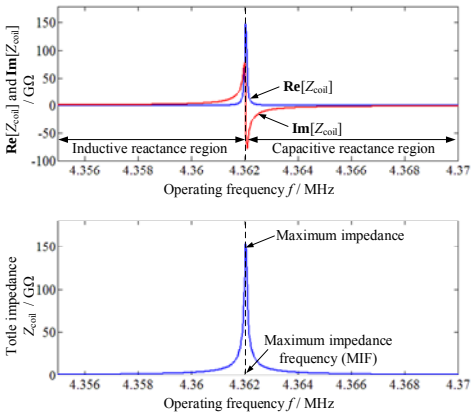

Fig. 5. Coil impedance curve on operating frequency.

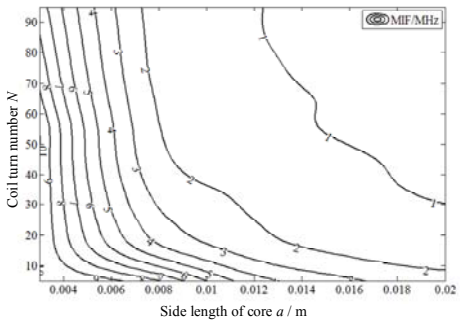

Fig. 6. Contour plot of the maximum impedance frequency.

B. Interference Isolation

For a power transfer with a low operating angular frequency ω_p, the impedances Z_{t1} and Z_{r1} can be expressed as:

$$\begin{cases} Z_{t1}(\omega_p) = j\omega_p L_{t1}(\omega_p) + R_{t1}(\omega_p) \\ Z_{r1}(\omega_p) = j\omega_p L_{r1}(\omega_p) + R_{r1}(\omega_p) \end{cases} \tag{9}$$

where $j\omega_p L_{t1}$ and $j\omega_p L_{r1}$ represent the imaginary parts of Z_{t1} and Z_{r1}, and R_{t1} and R_{r1} indicate the real parts. To compensate for the big reactance of the capacitive coupling structure C_{s1} and C_{s2}, the following equation should be satisfied:

$$\omega_p^2\left(L_{t1}(\omega_p) + L_{r1}(\omega_p)\right)\frac{C_{s1}C_{s2}}{C_{s1}+C_{s2}} = 1 \tag{10}$$

In addition, to keep the data carrier transferring through data branches, the MIF points of the impedances Z_{t1} and Z_{r1} should be set on the data carrier frequency as:

$$MIF(Z_{t1}) = \frac{\omega_d}{2\pi}, \quad MIF(Z_{r1}) = \frac{\omega_d}{2\pi} \tag{11}$$

For each of the impedance modules Z_{t2} and Z_{r2}, to isolate the power interference, a coil whose MIF point is set on the power carrier angular frequency ω_p is adopted. It is obvious that the impedance of this coil is a capacitive reactance at the data carrier frequency according to Fig. 5. Therefore, another coil connected in series with the former coil is needed. The MIF point of the second coil is set to a frequency that is higher than ω_p so that its impedance presents an inductive reactance at the frequency ω_p, which compensates the capacitive reactance at a high data carrier angular frequency and enhances the data carrier gain. As a result, the impedances Z_{t2} and Z_{r2} are divided between the two coils, respectively. Therefore, the impedances Z_{t2} and Z_{r2} can be expressed as:

$$\begin{cases} Z_{t2}(\omega_d) = j\omega_d L_{t2}(\omega_d) + 1/j\omega_d C_{t2}(\omega_d) + R_{t2}(\omega_d) \\ Z_{r2}(\omega_d) = j\omega_d L_{r2}(\omega_d) + 1/j\omega_d C_{r2}(\omega_d) + R_{r2}(\omega_d) \end{cases} \tag{12}$$

where $1/j\omega_d C_{r2}$ and $1/j\omega_d C_{t2}$ represent the capacitive reactance of Z_{t2} and Z_{r2}, and $j\omega_d L_{r2}$ and $j\omega_d L_{t2}$ indicate the inductive reactance of Z_{t2} and Z_{r2}. In addition, the impedances should satisfy the following constraints:

$$\begin{cases} \omega_d^2 L_{t2}(\omega_d) C_{t2}(\omega_d) = 1, \quad \omega_d^2 L_{r2}(\omega_d) C_{r2}(\omega_d) = 1 \\ MIF(Z_{t2}) = \dfrac{\omega_p}{2\pi}, \quad MIF(Z_{r2}) = \dfrac{\omega_p}{2\pi} \end{cases} \tag{13}$$

TABLE I
THE INHERENT PARAMETERS OF COILS

Parameters	Values	Parameters	Values
ε_0	8.85×10^{-12}F/m	h	1.1mm
r	1mm	d	5mm
ρ	$1.75\times10^{-8}\Omega$m	$\mu_0\mu_r$	$400\pi\times10^{-8}$H/m

V. SIMULATION AND EXPERIMENTS

In order to verify the above theoretical analysis, simulations and experiments are conducted in MATLAB based on the circuit shown in Fig. 2 and Fig. 3(b). The power and data carrier frequencies are set to 1MHz and 9MHz, respectively. The geometrical parameters of the designed coils are designed according to the theory in Section IV.

A. Coil Impedance Characteristic

The inherent parameters of the designed coils and some of the physical constants are given by Table I.

According to the analysis in Section IV, the side length of the core section and the coil turns are set as (a=6mm, N=11), (a=3mm, N=16) and (a=20mm, N=32), respectively. The impedance value for each of the coils is calculated and given in Table II under both the power and data carrier frequencies operating conditions.

Fig. 7 shows the impedance characteristic curves of the coils in the frequency domain over the operating frequency range from 0MHz to 15MHz. From Fig. 7, it can be seen that the MIF of coil Z_1 is set to f_d which can be used to keep the data carrier transferring in the data branches. In addition, the MIF of $Z_2^{(c)}$ is around f_p, which isolates the power interference. $Z_2^{(L)}$ is adopted to compensate the impedances of $Z_2^{(c)}$ under the f_d condition.

B. Interference Isolation Characteristic

The circuit parameters, not including the coils analyzed above, are given in Table III. Moreover, the curves of the gain functions established in Section II to estimate the power interference on the signal transmission and the voltage gain

TABLE II
THE GEOMETRICAL PARAMETERS AND THE IMPEDANCE VALUES OF COILS

Z_{t1},Z_{r1}(a=6mm, N=8)				$Z_{t2}^{(L)}$, $Z_{r2}^{(L)}$ (a=6mm, N=5)				$Z_{t2}^{(C)}$, $Z_{r2}^{(C)}$ (a=20mm, N=32)			
Power ω_p		Data ω_d		Power ω_p		Data ω_d		Power ω_p		Data ω_d	
L_{t1}	39.5μH	C_{t1}	0.5pF	L_{t2}	15.3μH	L_{t2}	43.3μH	C_{t2}	1.2pF	C_{t2}	7.3pF
R_{t1}	0.8Ω	R_{t1}	26.3kΩ	$R_{t2}^{(L)}$	0.2Ω	$R_{t2}^{(L)}$	120.2Ω	$R_{t2}^{(L)}$	226.7kΩ	$R_{t2}^{(L)}$	19.4Ω
L_{r1}	39.5μH	C_{r1}	0.5pF	L_{r2}	15.3μH	L_{r2}	43.3μH	C_{r2}	1.2pF	C_{t2}	7.3pF
R_{r1}	0.8Ω	R_{r1}	26.3kΩ	$R_{r2}^{(L)}$	0.2Ω	$R_{r2}^{(L)}$	120.2Ω	$R_{t2}^{(L)}$	226.7kΩ	$R_{t2}^{(L)}$	19.4Ω

TABLE III
CIRCUIT PARAMETERS BESIDE THE COILS

Parameters	Values	Parameters	Values
C_{s1}	650pF	C_{s2}	650pF
R_{td}	200Ω	R_{rd}	200Ω
f_d	9MHz	f_p	1MHz
R_{ac}	100Ω	u_p(Vpp)	200V
u_d(Vpp)	10V		

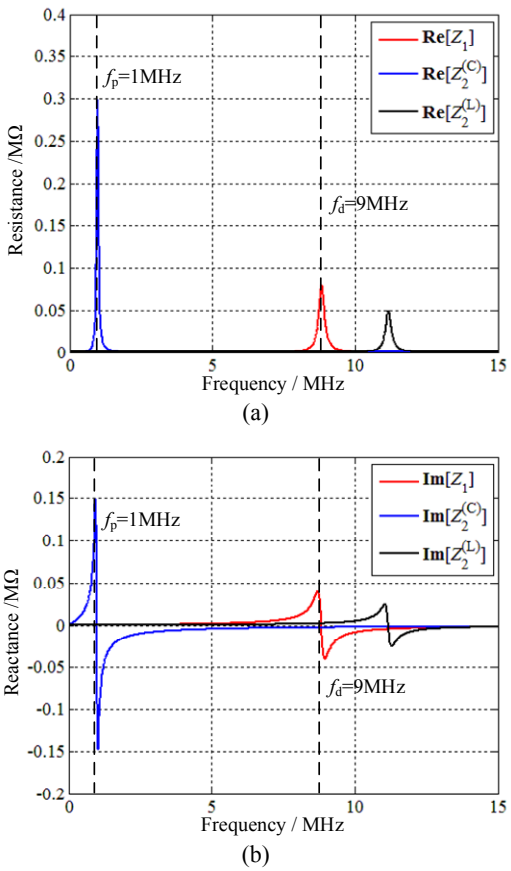

Fig. 7. Coils impedance characteristic in frequency domain.

of the data carrier are illustrated in Fig. 8. The measured voltage gain values in the experiments are shown in Fig. 8 as circles at each of the measured frequencies.

In Fig. 8(a), the function curves of $20\lg G_{int\text{-}tr}$ and $20\lg G_{int\text{-}rt}$ show that the power attenuation from the power input port to the data sensing resistors R_{td} and R_{rd} are both around -45dB under the f_p condition. Although the experimental values

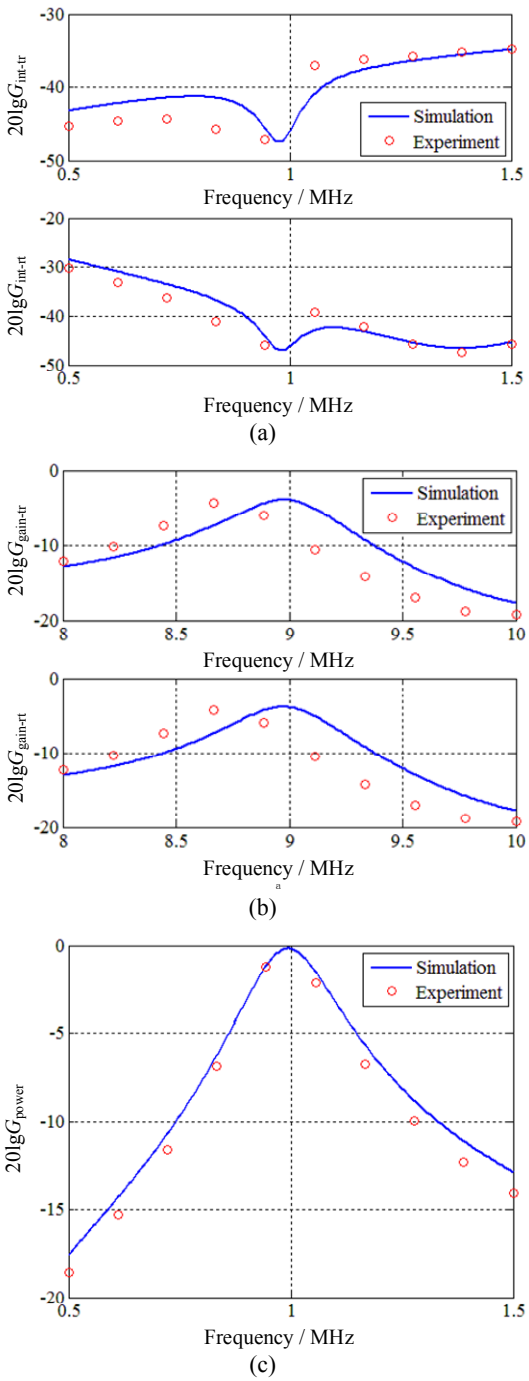

Fig. 8. Simulated and experimental results of the proposed method.

deviate slightly from the simulated curves, the power attenuation level on f_p is still acceptable. In Fig. 8(b), the function curves of $20\lg G_{gain\text{-}tr}$ and $20\lg G_{gain\text{-}rt}$ show that the data carrier attenuation from the data input port to the data sensing resistors R_{td} and R_{rd} are both smaller than -5dB under the f_d condition which is practical for data transmission. Here, the peaks of these two function curves in practical experiments appear at 8.7MHz, which is pretty close to the designed frequency 9MHz. In Fig. 8(c), the power attenuation from the power input port to the load is nearly 0dB. The experimental results have some small differences when compared with the simulations as a result of the measurement errors of actual geometric dimensioning and the parameter changes due to temperature drift, etc. Therefore, the practical data carrier frequency and the voltage gains of the power and crosstalk are slightly different from the theoretical values. The experimental results are consistent with simulations.

VI. Conclusion

In this paper, a novel interference isolation method is proposed by using several designed coils in a capacitive power transfer system as isolation impedances. For each designed coil, its stray parameters such as the inter-turn capacitance, the coil resistance and the capacitance between the coil and core, etc. are taken into account. According to the equivalent circuit of the designed coils, the impedance characteristics of these coils are given. In addition, the maximum impedance point and the corresponding excitation frequency of the coil are obtained. Based on the above analysis, six designed coils are adopted to isolate the interference from power delivery. The power and data carriers with frequencies of 1MHz and 8.7MHz are transferred in parallel. Moreover, the data carrier attenuation is lower than -5dB, and the power attenuation on the sensing resistor is higher than -45dB.

Appendix

To analyze the power and data transfer characteristics of the proposed WPST system, five corresponding functions are shown as Eq.(14) to Eq.(18).

where $C_s = C_{s1}C_{s2}/(C_{s1}+C_{s2})$, and ω_p and ω_d represent the angular frequencies of the power carrier and data carrier, respectively. The variable $Z_x^{(\omega)}$ indicates the impedance of module x under operating frequencies of ω, which are marked as a superscript. All of the equations from Eq.(14) to Eq.(18) are obtained based on the Fundamental Harmonic Analysis (FHA) method according to the circuit in Fig. 3(b).

$$G_{int\text{-}tr}=\left|\frac{R_{rd}}{R_{rd}+Z_{r2}^{(\omega_p)}}\cdot\frac{\left(\left(Z_{r1}^{(\omega_p)}+R_{ac}\right)\|\left(Z_{r2}^{(\omega_p)}+R_{rd}\right)+\frac{1}{j\omega_p C_s}\right)\|Z_{t2}^{(\omega_p)}}{\left(\left(Z_{r1}^{(\omega_p)}+R_{ac}\right)\|\left(Z_{r2}^{(\omega_p)}+R_{rd}\right)+\frac{1}{j\omega_p C_s}\right)\|Z_{t2}^{(\omega_p)}+Z_{t1}^{(\omega_p)}}\cdot\frac{\left(Z_{r1}^{(\omega_p)}+R_{ac}\right)\|\left(Z_{r2}^{(\omega_p)}+R_{rd}\right)}{\left(Z_{r1}^{(\omega_p)}+R_{ac}\right)\|\left(Z_{r2}^{(\omega_p)}+R_{rd}\right)+\frac{1}{j\omega_p C_s}}\right| \tag{1}$$

$$G_{int\text{-}rt}=\left|\frac{R_{td}}{R_{td}+Z_{t2}^{(\omega_p)}}\cdot\frac{\left(\left(Z_{r1}^{(\omega_p)}+R_{ac}\right)\|Z_{r2}^{(\omega_p)}+\frac{1}{j\omega_p C_s}\right)\|\left(Z_{t2}^{(\omega_p)}+R_{td}\right)}{\left(\left(Z_{r1}^{(\omega_p)}+R_{ac}\right)\|Z_{r2}^{(\omega_p)}+\frac{1}{j\omega_p C_s}\right)\|\left(Z_{t2}^{(\omega_p)}+R_{td}\right)+Z_{t1}^{(\omega_p)}}\right| \tag{2}$$

$$G_{gain\text{-}tr}=\left|\frac{R_{rd}}{R_{rd}+Z_{r2}^{(\omega_d)}}\cdot\frac{\left(\left(Z_{r1}^{(\omega_d)}+R_{ac}\right)\|\left(Z_{r2}^{(\omega_d)}+R_{rd}\right)+\frac{1}{j\omega_d C_s}\right)\|Z_{t1}^{(\omega_d)}}{\left(\left(Z_{r1}^{(\omega_d)}+R_{ac}\right)\|\left(Z_{r2}^{(\omega_d)}+R_{rd}\right)+\frac{1}{j\omega_d C_s}\right)\|Z_{t1}^{(\omega_d)}+Z_{t2}^{(\omega_d)}}\cdot\frac{\left(Z_{r1}^{(\omega_d)}+R_{ac}\right)\|\left(Z_{r2}^{(\omega_d)}+R_{rd}\right)}{\left(Z_{r1}^{(\omega_d)}+R_{ac}\right)\|\left(Z_{r2}^{(\omega_d)}+R_{rd}\right)+\frac{1}{j\omega_d C_s}}\right| \tag{3}$$

$$G_{gain\text{-}rt}=\left|\frac{R_{td}}{R_{td}+Z_{t2}^{(\omega_d)}}\cdot\frac{\left(\left(Z_{t2}^{(\omega_d)}+R_{td}\right)\|Z_{t1}^{(\omega_d)}+\frac{1}{j\omega_d C_s}\right)\|\left(Z_{r1}^{(\omega_d)}+R_{ac}\right)}{\left(\left(Z_{t2}^{(\omega_d)}+R_{td}\right)\|Z_{t1}^{(\omega_d)}+\frac{1}{j\omega_d C_s}\right)\|\left(Z_{r1}^{(\omega_d)}+R_{ac}\right)+Z_{r2}^{(\omega_d)}}\cdot\frac{\left(Z_{t2}^{(\omega_d)}+R_{td}\right)\|Z_{t1}^{(\omega_d)}}{\left(Z_{t2}^{(\omega_d)}+R_{td}\right)\|Z_{t1}^{(\omega_d)}+\frac{1}{j\omega_d C_s}}\right| \tag{4}$$

$$G_{power}=\left|\frac{R_{ac}}{R_{ac}+Z_{r1}^{(\omega_p)}}\cdot\frac{\left(\left(Z_{r1}^{(\omega_p)}+R_{ac}\right)\|\left(Z_{r2}^{(\omega_p)}+R_{rd}\right)+\frac{1}{j\omega_p C_s}\right)\|Z_{t2}^{(\omega_p)}}{\left(\left(Z_{r1}^{(\omega_p)}+R_{ac}\right)\|\left(Z_{r2}^{(\omega_p)}+R_{rd}\right)+\frac{1}{j\omega_p C_s}\right)\|Z_{t2}^{(\omega_p)}+Z_{t1}^{(\omega_p)}}\cdot\frac{\left(Z_{r1}^{(\omega_p)}+R_{ac}\right)\|\left(Z_{r2}^{(\omega_p)}+R_{rd}\right)}{\left(Z_{r1}^{(\omega_p)}+R_{ac}\right)\|\left(Z_{r2}^{(\omega_p)}+R_{rd}\right)+\frac{1}{j\omega_p C_s}}\right| \tag{5}$$

ACKNOWLEDGMENT

This work was sponsored by the research funds for the National Natural Science Foundation of China under Grants #51477020. This work was also supported by Chongqing International Science and Technology Cooperation Base Project under Grants CSTC2015GJHZ40001.

REFERENCE

[1] J. H. Kim, B. Lee, J. Lee, S. Lee, C. Park, S. Jung, S. Lee, K. Yi, and J. Baek, "Development of 1-MW inductive power transfer system for a high-speed train," *IEEE Trans. Ind. Electron.*, Vol. 62, No. 10, pp. 6242-6250, Oct. 2015.

[2] Y. Su, H. Zhang, Z. Wang, A. P. Hu, L. Chen, and Y. Sun, "Steady-state load identification method of inductive power transfer system based on switching capacitors," *IEEE Trans. Power Electron.*, Vol. 30, No. 11, pp. 6349-6355, Nov. 2015.

[3] J. Huh, W. Lee, S. Choi, G. Cho, and C. Rim, "Frequency-domain circuit model and analysis of coupled magnetic resonance systems," *Journal of Power Electronics*, Vol. 13, No. 2, pp. 275-286, Mar. 2013.

[4] X. Dai, Y. Zou, and Y. Sun, "Uncertainty modeling and robust control for LCL resonant inductive power transfer system," *Journal of Power Electronics*, Vol. 13, No. 5, pp. 814-828, Sep. 2013.

[5] J. Dai and D. C. Ludois, "A survey of wireless power transfer and a critical comparison of inductive and capacitive coupling for small gap applications," *IEEE Trans. Power Electron.*, Vol. 30, No. 11, pp. 6017-6029, Nov. 2015.

[6] L. Huang and A. P. Hu, "Defining the mutual coupling of capacitive power transfer for wireless power transfer," *Electronics Letters*, Vol. 51, No. 22, pp. 1806-1807, Oct. 2015.

[7] M. P. Theodoridis, "Effective capacitive power transfer," *IEEE Trans. Power Electron.*, Vol. 27, No. 12, pp. 4906-4913, Dec. 2012.

[8] C. Liu, A. P. Hu, and N. K. C. Nair, "Modelling and analysis of a capacitively coupled contactless power transfer system," *IET Power Electronics*, Vol. 4, No. 7, pp. 808-815, Aug. 2011.

[9] D. C. Ludois, M. J. Erickson, and J. K. Reed, "Aerodynamic fluid bearings for translational and rotating capacitors in noncontact capacitive power transfer systems," *IEEE Trans. Ind. Appl.*, Vol. 50, No. 2, pp. 1025-1033, Mar./Apr. 2014.

[10] A. P. Hu, C. Liu, and H. L. Li, "A novel contactless battery charging system for soccer playing robot," in *International Conference on Mechatronics and Machine Vision in Practice*, pp. 623-627, 2008.

[11] A. I. Al-Kalbani, M. R. Yuce, and J. Redoute, "A biosafety comparison between capacitive and inductive coupling in biomedical implants," *IEEE Antennas and Wireless Propagation Letters*, Vol. 13, No. 1, pp. 1168-1171, Jun. 2014.

[12] B. H. Choi, D. T. Nguyen, S. J. Yoo, J. H. Kim, and C. T. Rim, "A novel source-side monitored capacitive power transfer system for contactless mobile charger using Class-E converter," in *Vehicular Technology Conference*, pp. 1-5, 2014.

[13] F. Lu, H. Zhang, H. Hofmann, and C. Mi, "A double-sided LCLC-compensated capacitive power transfer system for electric vehicle charging," *IEEE Trans. Power Electron.*, Vol. 30, No. 11, pp. 6011-6014, Nov. 2015.

[14] J. Dai and D. C. Ludois, "Wireless electric vehicle charging via capacitive power transfer through a conformal bumper," in *Applied Power Electronics Conference and Exposition*, pp. 3307-3313, 2015.

[15] C. Liu, A. P. Hu, B. Wang, and N. C. Nair, "A capacitively coupled contactless matrix charging platform with soft switched transformer control," *IEEE Trans. Ind. Electron.*, Vol. 60, No. 1, pp. 249-260, Jan. 2013.

[16] Y. Su, S. Xie, A. Hu, C. Tang, and W. Zhou, "Transmission property analysis of electric-field coupled wireless power transfer system with LCL resonant network," *Transactions of China Electrotechnical Society*, Vol. 30, No. 19, pp. 55-60, Oct. 2015.

[17] H. L. Li, A. P. Hu, and G. A. Covic, "Primary current generation for a contact less power transfer system using free oscillation and energy injection control," *Journal of Power Electronics*, Vol. 11, No. 3, pp. 256-263, May 2011.

[18] G. Wang, P. Wang, Y. Tang, and W. Liu, "Analysis of dual band power and data telemetry for biomedical implants," *IEEE Trans. Biomed. Circuits Syst.*, Vol. 6, No. 3, pp. 208-215, Jun. 2012.

[19] Y. Su, W. Zhou, A. Hu, Y. Sun, and L. Chen, "A power-signal parallel transmission technology for ECPT systems based on duty cycle modulation of square wave carrier," *Transactions of China Electrotechnical Society*, Vol. 30, No. 21, pp. 51-56, Nov. 2015.

[20] J. Wu, C. Zhao, J. Du, Z. Lin, Y. Hu, and X. He, "Wireless power and data transfer via a common inductive link using frequency division multiplexing," *IEEE Trans. Ind. Electron.*, Vol. 62, No. 12, pp. 7810-7820, Dec. 2015.

[21] J. Hirai, T. Kim, and A. Kawamura, "Integral motor with driver and wireless transmission of power and information for autonomous subspindle drive," *IEEE Trans. Power Electron.*, Vol. 15, No. 1, pp. 13-20, Jan. 2000.

[22] R. L. Steigerwald, "A comparison of half-bridge resonant converter topologies," *IEEE Trans. Power Electron.,* Vol. 3, No. 2, pp. 174-182, Apr. 1988.

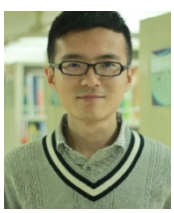

Wei Zhou received his B.E. degree from the College of Automation of Chongqing University, Chongqing, China, in 2013, where he is presently working towards his Ph.D. degree in Control Theory and Control Engineering. He is presently a Visiting Scholar in the Department of Electrical and Computer Engineering, University of Auckland, Auckland, New Zealand. His current research interests include capacitive power transfer technology, wireless power, signal parallel transmissions and control theory.

Yu-Gang Su received his B.E. and M.E. degrees in Industrial Automation and his Ph.D. degree in Control Theory and Control Engineering from Chongqing University, Chongqing, China, in 1985, 1993 and 2004, respectively. From 2008 to 2009, he was a Visiting Scholar at the University of Queensland, Brisbane, Australia. He is presently working as a Professor in the College of Automation, Chongqing University. His current research interests include power electronics, control theory and applications, and wireless power transfer.

Shi-Yun Xie received his B.E. degree from the College of Automation of Chongqing University, Chongqing, China, in 2010, where he is presently working towards his Ph.D. degree in Control Theory and Control Engineering. His current research interests include the mixed-resonant topologies of capacitive power transfer systems and their control strategies, and wireless power transfer technologies.

Long Chen received his B.E. degree in Medial Information from the Southern Medical University, Guangzhou, China, in 2011. He is presently working towards his Ph.D. degree in Control Theory and Control Engineering in the College of Automation, Chongqing University, Chongqing, China. His current research interests include load identification and the optimization of wireless power transfer systems.

Xin Dai received his B.E. degree in Industrial Automation from Yuzhou University, Chongqing, China, in 2000; and his Ph.D. degree in Control Theory and Control Engineering from the School of Automation, Chongqing University, Chongqing, China, in 2006. In 2012, he was a Visiting Scholar at the University of Auckland, Auckland, New Zealand. He is presently working as a Professor in the School of Automation, Chongqing University. His current research interests include inductive power transfer technologies and the nonlinear dynamic behaviour analysis of power electronics.

Yu-Ming Zhao received his B.E. degree from the College of Automation of Chongqing University, Chongqing, China, in 2014, where he is presently working towards his Ph.D. degree in the Control Theory and Control Engineering. His current research interests include capacitively coupled power transfer and its modelling.